Materials Today Bio 15 (2022) 100316

Contents lists available at ScienceDirect

Materials Today Bio

journal homepage: www.journals.elsevier.com/materials-today-bio

Synthesis of a versatile mitochondria-targeting small molecule for cancer near-infrared fluorescent imaging and radio/photodynamic/photothermal synergistic therapies

Mingquan Gao [a,b], Xie Huang [c], Zifei Wu [a,b], Liting Wang [d], Shaolong Yuan [d], Zaizhi Du [d], Shenglin Luo [c], Rong Li [c,**], Weidong Wang [a,b,*]

[a] School of Medicine, University of Electronic Science and Technology of China, Chengdu, Sichuan, 610054, China
[b] Department of Radiation Oncology, Sichuan Cancer Hospital, Sichuan Key Laboratory of Radiation Oncology, School of Medicine, University of Electronic Science and Technology of China, Chengdu, Sichuan, 610041, China
[c] State Key Laboratory of Trauma, Burns and Combined Injury, Institute of Combined Injury, Chongqing Engineering Research Center for Nanomedicine, College of Preventive Medicine, Third Military Medical University (Army Medical University), Chongqing, 400038, China
[d] Biomedical Analysis Center, Third Military Medical University (Army Medical University), Chongqing, 400038, China

ARTICLE INFO

Keywords:
Radiotherapy
Phototherapy
Radiosensitizer
Near-infrared imaging
Heptamethine cyanine dyes

ABSTRACT

Although as a mainstay modal for cancer treatment, the clinical effect of radiotherapy (RT) does not yet meet the need of cancer patients. Developing tumour-preferential radiosensitizers or combining RT with other treatments has been acknowledged highly necessary to enhance the efficacy of RT. The present study reported a multi-functional bioactive small-molecule (designated as IR-83) simultaneously exhibiting tumour-preferential accumulation, near-infrared imaging and radio/photodynamic/photothermal therapeutic effects. IR-83 was designed and synthesized by introducing 2-nitroimidazole as a radiosensitizer into the framework of heptamethine cyanine dyes inherently with tumour-targeting and photosensitizing effects. As results, IR-83 preferentially accumulated in tumours, suppressed tumour growth and metastasis by integrating radio/photodynamic/photothermal multi-modal therapies. Mechanism studies showed that IR-83 accumulated in cancer cell mitochondria, induced excessive reactive oxygen species (ROS), and generated high heat after laser irradiation. On one hand, these phenomena led to mitochondrial dysfunction and a sharp decline in oxidative phosphorylation to lessen tissue oxygen consumption. On the other hand, excessive ROS in mitochondria destroyed the balance of antioxidants and oxidative stress balance by down-regulating the intracellular antioxidant system, and subsequently sensitized ionizing radiation-generated irreversible DNA double-strand breaks. Therefore, this study presented a promising radiosensitizer and a new alternative strategy to enhance RT efficacy via mitochondria-targeting multimodal synergistic treatment.

1. Introduction

RT is one of the most routinely used therapeutic modalities for cancer patients, and >75% of non-small cell lung cancer (NSCLC) patients have received this treatment [1]. Mechanistically, high-energy radiation (X-ray, β-ray, or γ-ray) directly react with the cellular aqueous environment and generates reactive ROS, which ultimately result in DNA double-strand breaks (DSBs) [2]. Despite dramatic improvements in

Abbreviations: RT, radiotherapy; ROS, reactive oxygen species; NSCLC, non-small cell lung cancer; DSBs, DNA double-strand breaks; PDT, photodynamic therapy; PTT, photothermal therapy; PSs, photosensitizers; PTAs, photothermal agents; NIR, near-infrared; OXPHOS, oxidative phosphorylation; NMR, nuclear magnetic resonance; LLC, Lewis lung carcinoma; CLSM, confocal laser scanning microscope; PI, propidium iodide; SOSG, Singlet oxygen sensor green; PBS, phosphate-buffered saline; SER, sensitizer enhancement ratio; MMP, mitochondrial membrane potential; GSH, glutathione; Nrf2, nuclear factor erythroid-derived 2-like 2; HO-1, heme oxygenase 1; NADPH, nicotinamide adenine dinucleotide phosphate; H&E, hematoxylin and eosin; CREA, creatinine; ALT, alanine aminotransferase; AST, aspartate amino transferase; WBC, white blood cell; RBC, red blood cell; PLT, Platelet.

* Corresponding author. No. 55, section 4, Renmin South Road, Chengdu, Sichuan Province, China.
** Corresponding author. No. 30, Gaotanyan Zheng Street, Shapingba District, Chongqing, China.
E-mail addresses: lirongwd@tmmu.edu.cn (R. Li), wwdwyl@uestc.edu.cn (W. Wang).

https://doi.org/10.1016/j.mtbio.2022.100316
Received 20 April 2022; Received in revised form 1 June 2022; Accepted 3 June 2022
Available online 7 June 2022

radiation therapy, the clinical benefits are not yet satisfactory due to inherent and acquired radiation resistance, DNA self-repair mechanism, as well as side effects to normal tissues [3]. Notably, the existence of a hypoxia environment in solid tumours greatly limits the therapeutic efficacy of RT, thus leading to radio-resistance or treatment failure [4]. A large number of studies have been devoted to improving the RT efficacy via developing radiosensitizers or combining RT with other therapeutic modalities [5–7].

In recent decades, phototherapy has shown a significant application prospect in tumour treatment owing to its non-invasiveness, spatiotemporal selectivity and low side effects [8]. Phototherapeutic agents act on tumour cells through two distinct treatment modalities, photodynamic therapy (PDT) and photothermal therapy (PTT). In PDT, photosensitizers (PSs) absorb energy from light and sensitize tissue oxygen to generate a variety of ROS, including singlet oxygen ($^1O_2$), superoxide anion radical ($O^{2\bullet-}$), hydrogen peroxide (H_2O_2) and hydroxyl radical (HO·) [9]. The excessive cytotoxic ROS produced from PDT significantly enhances the RT efficacy by amplifying DNA DSBs [10]. RT combined with PDT treatment is valuable to overcome the deficiency of PDT with respect to poor tissue penetration of light radiation [11]. In PTT, photothermal agents (PTA), such as carbon nanomaterials and gold nanomaterials, cause thermal ablation of the adjacent cells by converting light energy into hyperthermia [12,13]. PTT is considered as an oxygen-independent cancer therapy, so it is an ideal supplement to RT or PDT. Especially, recent studies have revealed that hyperthermia improves tumour blood flow and increases the perfused fraction of the tumour, which subsequently increases vascular permeability and tumoral O_2 level and decreases the interstitial fluid pressure [14–16]. These alternations exert a positive impact on RT. Several clinical trials also have confirmed that combining hyperthermia with RT leads to favorable efficacies on local tumour control, long-term free survival, and complete remission in various solid malignancies [17,18].

To maximize the improvement of RT efficacy, a few multifunctional nanomaterials have recently been fabricated to integrate ionizing irradiation and dual-modal phototherapies (PDT and PTT) [19–21]. Triple therapy has been deemed as a feasible strategy to eradicate tumours synergistically, based on the impressive results from the published reports. Nevertheless, nanomaterial-based agents are faced with several fundamental problems, indicating that most of them are still in the early stage of proof of concept [22–24]. In our previous work, a series of multifunctional small-molecule heptamethine indocyanine dyes have been reported for tumour-preferential near-infrared (NIR) imaging, chemotherapy [25], PDT [26], PDT/PTT [27], chemo-/PDT/PTT [28], and chemo-radiotherapy [29]. In this work we will present a new analogue (IR-83) of heptamethine indocyanine dyes for tumour-targeting, NIR imaging, and RT/PDT/PTT. IR-83 was designed and synthesized by introducing 2-nitroimidazole (as a radiosensitizer moiety) into the framework of heptamethine cyanine dyes that have been established with excellent tumour-targeting and PDT/PTT photosensitizing effects. This design offered a new multifunctional small molecule with tumour-preferential accumulation and imaging-guided RT/PDT/PTT locally precise treatment. More importantly, IR-83 accumulated in cancer cell mitochondria and exerted a synergistic therapeutic effect of RT/PDT/PTT by targeting mitochondria. Regarding the major roles of mitochondria on cancer cell survival and metastasis, IR-83 induces a sharp decline in oxidative phosphorylation (OXPHOS) to lessen tissue oxygen consumption and a remarkable increase in ROS level to sensitize RT. To the best of our knowledge, this is the first report of a therapeutic small molecule integrating RT/PDT/PTT triple treatment by targeting cancer cell mitochondria, which might present a practicable strategy to develop small-molecule-based cancer theranostic agents for simultaneous cancer targeting, imaging and therapy.

2. Results and discussion

2.1. Synthesis and characterization of IR-83

IR-83 was synthesized via a five-step reaction by introducing a hypoxia-affinity nitroimidazole and a hydrophilic sulfonic group, respectively, into the framework of heptamethine cyanine dyes (Scheme 1). The successful synthesis of IR-83 was confirmed by ^1H nuclear magnetic resonance (NMR), ^{13}C NMR, and high-resolution mass spectrometry (Figure S1-S6). We next characterized the photophysical properties of IR-83 in various solvents. UV–vis–NIR spectrum analysis showed the maximal absorbance peak of IR-83 in different solvents located at 782–797 nm (Figure S7A). In addition, the maximal excitation/emission wavelength of IR-83 in $CHCl_3$ located at 763/816 nm (Figure S7B). It's generally accepted that near-infrared fluorescent dyes with high Stokes shift (more than 20 nm) are hence conducive to imaging and sensing [30]. IR-83 exhibits relatively excellent Stokes shift (Table S1) in various solvents and therefore considering as a candidate fluorescent probe for bio-imaging.

2.2. Cellular uptake and hypoxic tumour targeting of IR-83

We then evaluated the cellular uptake properties of IR-83 and results revealed that cellular fluorescence signals (red) in LLC cells were gradually elevated with the increase in time until 8 h (Fig. 1A and Figure S8A), indicating that the cell internalization of IR-83 occurs in the cytoplasm in a time-dependent manner. By virtue of the hypoxia-affinity

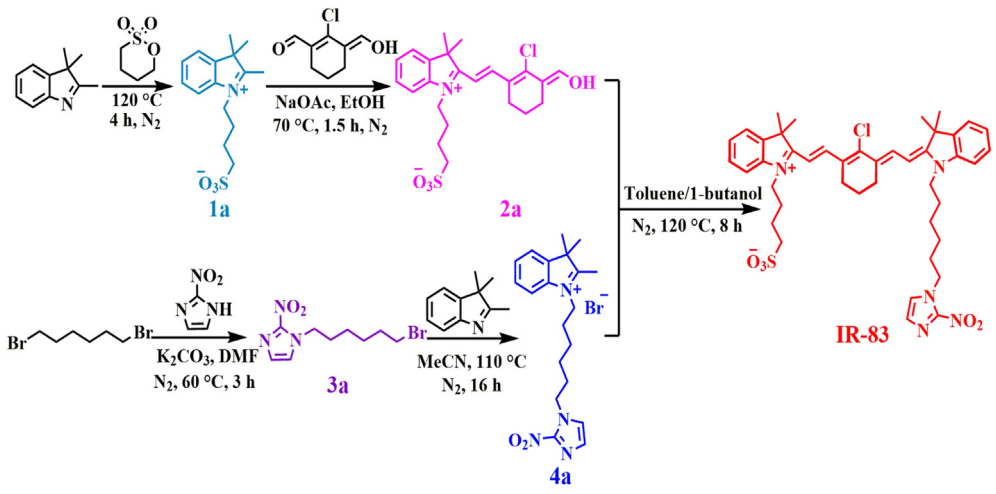

Scheme 1. Structure and synthetic route of IR-83.

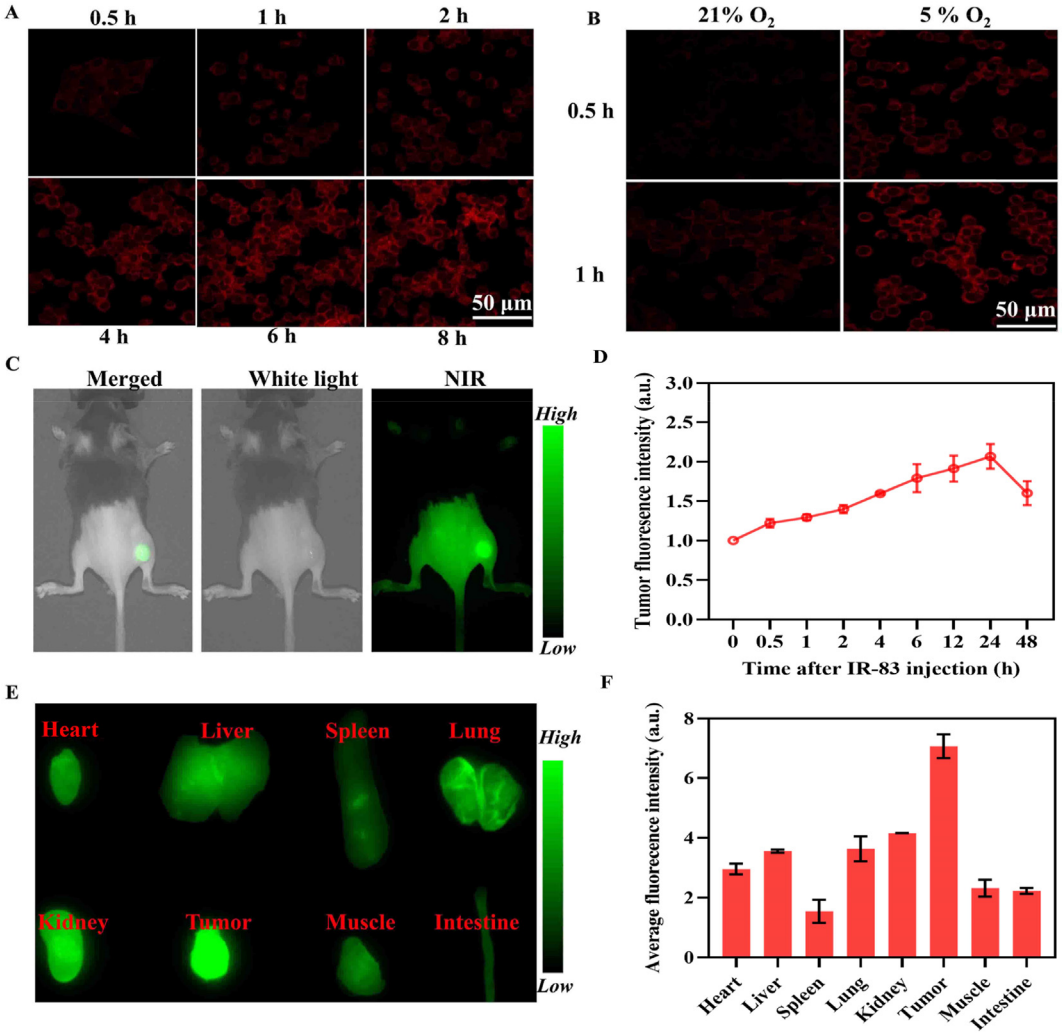

Fig. 1. In vivo and ex vivo fluorescence imaging properties of IR-83. Real-time confocal fluorescence images of LLC cells after treatment with (A) IR-83 (2.5 μM) for different durations or B) incubated at normoxic (21% O_2) or hypoxic (5% O_2) condition. (C) *In vivo* fluorescence images of tumour-bearing mice taken at 24 h after -intravenous injection of IR-83 (0.25 mg/kg). (D). Quantitation of fluorescence intensities of the tumour areas after IR-83 intravenous injection (n = 3). (E) *Ex vivo* fluorescence images of major organs and tumours dissected from LLC tumour-bearing mice at 24 h after intravenous injection of IR-83. (F) Semi-quantitative analysis of the average fluorescence intensities from excised tumour and vital organs (heart, liver, spleen, lung, and kidney) at 24 h post-IR-83 injection. The fluorescence intensity of intestine was served as reference to calculate relative fluorescence intensity of other organs.

characteristic of nitroimidazole chemical group [31], IR-83 was speculated to possess the ability of hypoxia-preferential accumulation. In order to substantiate our design, the uptake of IR-83 in LLC cells cultured in an anaerobic incubator (5% O_2) was compared to the cells cultured under normal conditions (21% O_2). As expected, the cellular uptake of IR-83 in hypoxic conditions was significantly higher than that in normoxic conditions (Fig. 1B and Figure S8B). These results demonstrated that IR-83 could preferentially accumulated in tumour cells under the existence of hypoxia tumour microenvironment.

Next, the tumour-targeting property and *in vivo* bioimaging potential of IR-83 were assessed using a NIR small animal imaging system. *In vivo* NIR imaging displayed a strong fluorescence signal in the tumour region, indicating tumour-specific retention property of IR-83 (Fig. 1C). Apparently, the fluorescence signal of IR-83 in the tumour area was observed 0.5 h after injection and increased as time elapsed (Fig. 1D). The fluorescence intensity reached a peak at 24 h after injection (Figure S9). Then the ex vivo biodistribution of IR-83 in dissected organs (heart, liver, spleen, lung, kidney, muscle, intestine) and the tumour was evaluated at 24 h after injection. As shown in Fig. 1*E* and F, the tumour tissues displayed the strongest signals (from IR-83) than other organs, including reticuloendothelial systems such as liver and spleen, indicating the tumour preferential accumulation property of IR-83. In addition, IR-83 accumulated in the vital organs was reduced in a time-dependent manner and completely excreted out in both tumour-bearing mice and healthy mice at the 4th day after injection (Figure S10 and Figure S11A-C). Furthermore, it was found that the fluorescence intensity of IR-83 in blood samples were decreased by 48% until 24 h post injection, suggesting a long blood circulation time of IR-83 (Figure S11D). These findings indicated that the water-soluble IR-83 preferentially accumulated in tumours with rapid metabolism in body. Together with highly sensitive NIR fluorescent imaging property, IR-83 can be used to precisely kill tumours by distinguishing the tumours from their boundaries under imaging guidance.

2.3. PDT and PTT properties of IR-83

Before testifying the PDT and PTT effects of IR-83, we firstly examined the cytotoxicity of IR-83 against LLC cancer cells using a standard CCK-8 assay. As shown in Fig. 2A, cell viability analysis did not detect any cytotoxicity of IR-83 against LLC cells even at a high concentration up to 10 μM. Next, LLC cells were irradiated under 808 nm NIR laser (2 W/cm^2) for 5 min after incubation with 0–10 μM of IR-83 for 8 h. In

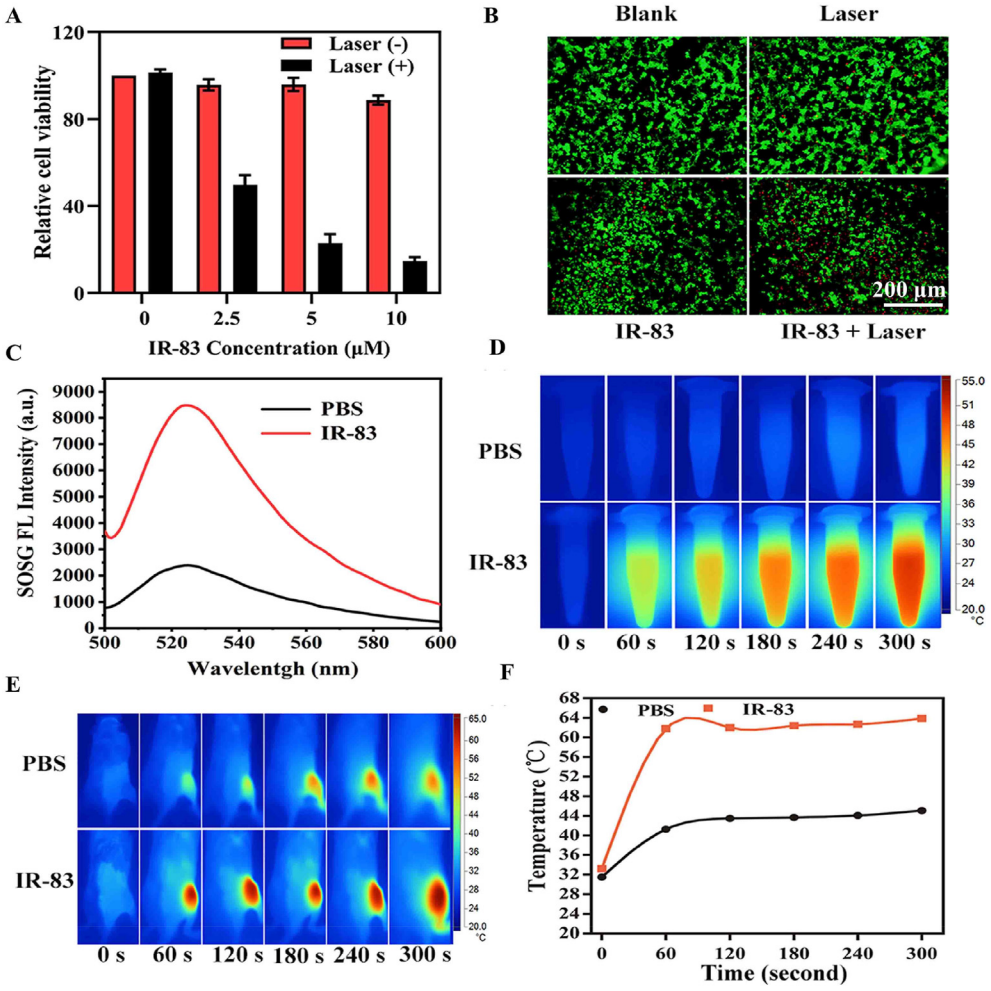

Fig. 2. PDT and PTT effects of IR-83 *in vitro* and *in vivo*. (A) Relative cell viability of LLC cells after incubation with gradient concentrations of IR-83 for 24 h in the absence or presence of 808 nm NIR laser irradiation (2 W/cm^2, 5 min). (B) Live/dead staining images of LLC cells after incubation with PBS or IR-83 in the absence or presence of 808 nm laser. Live and dead cells were labelled with Calcein-AM (green) and propidium iodide (red), respectively. (C). Quantification of the generation of singlet oxygen in PBS or IR-83 solution (2.5 μM) post-exposure to NIR laser (2 W/cm^2) for 5 min. (D) In vitro IR thermal images were recorded at different intervals in PBS (upper row) and IR-83 (2.5 μM) (lower row) groups under the presence of 808 nm laser (2 W/cm2). (E) Real-time IR thermal images of tumour-bearing mice post-intravenous injection of PBS or IR-83 (2.5 mg/kg) for 24 h under 808 nm laser (0.8 W/cm^2) irradiation. (F) Temperature cures of tumour surface in PBS or IR-83-injected mice upon continuous exposure to 808 nm laser.

contrast to non-irradiated cells with 100% cell viability, >50% of irradiated cells were killed when treated with 2.5 μM of IR-83. Therefore, the dosage of 2.5 μM was selected as the working concentration of IR-83 for *in vitro* experiment. Then, the phototherapeutic effect of IR-83 in LLC cells was tested at various NIR irradiation power densities. The results showed the killing efficacy of phototherapy against cancer cells that was augmented with increased laser power at the same concentration (Figure S12). Live/dead cell staining fluorescence images displayed bright green fluorescence in non-irradiated cells, while the strong red and weak green fluorescence was observed when cells were exposed to NIR irradiation (Fig. 2B and Figure S13), implying the effective phototherapeutic ablation of IR-83-stimulated LLC cells.

It has been widely acknowledged that phototherapeutic efficiency could be achieved through two distinct therapeutic patterns, PDT and PTT [32]. Therefore, we investigated whether IR-83 simultaneously served as a PS and PTA agent. As displayed in Fig. 2C, IR-83 alone only excited negligible fluorescence of Singlet oxygen sensor green (SOSG), whereas an obvious increase of the fluorescence intensity was observed when exposed to NIR laser, confirming the potential of IR-83 for cancer PDT therapy. It was found that the generation of SOSG was gradually reduced with decreasing oxygen concentration, indicating the photosensitization efficacy of IR-83 was oxygen-dependent (Figure S14). In addition, the *in vitro* IR thermal images illustrated that the temperature change was small in the control solution (maximum temperature: 29.4 °C). However, the temperature of IR-83 solution raised rapidly with prolonged duration and reached 54 °C at 5 min (Fig. 2D). The photothermal conversion efficiency (η) of IR-83 was calculated to be 54.1% (Figure S15). Regarding that many previously reported photothermal agents have a photothermal conversion efficiency below 50%, such as Au nanorods (36.7%) [33], $Cu_{2-X}Se$ (22%) nanocrystals [34], and Cu_9S_5 nanocrystals (25.7%) [35]. Apparently, compared with these well-known Au nanorods and typical semiconductors, IR-83 displays a considerably high photothermal efficiency.

One major obstacle that limits the clinical application of photosensitizer is the lack of tumour targeting, especially for hypoxic solid tumour [36], solutions to this problem in the PTT or PDT are required in order to broaden its clinical application. Inspired by the fascinating photothermal therapeutic efficacy and selective tumour accumulation properties of IR-83, an *in vivo* photothermal therapy study was then conducted on LLC subcutaneous tumour model. A slight temperature rise was observed in PBS-injected mice, which reached the maximum at ~40 °C. In contrast, for mice with IR-83 injection, the local temperature of the tumour surface was increased dramatically (ΔT ≈ 30 °C) in the first minute and was maintained at 60–65 °C in the remaining 4 min (Fig. 2*E* and F). These findings uncovered that IR-83 had a high photothermal conversion efficiency and could effectively transform light energy into regional heat, so it could exert an effective photothermal ablation effect on tumour cells inside the tumour region. Together, these findings indicated that IR-83 exhibited excellent phototherapeutic effect on LLC cells by functioning as dual-modal PDT and PTT agent.

2.4. *In vitro synergistic effect of IR-83-mediated RT/PDT/PTT*

Recently, integrating RT and phototherapy (single PDT or PTT in most cases) has become a hot topic for research and clinical experts, demonstrating that phototherapy has dramatically improved the RT

efficacy through targeting various aspects of cancer development, such as cell proliferation, metastasis and angiogenesis [37]. Based on previous literature, we explored whether RT in combination with phototherapy of IR-83 could offer synergetic therapeutic benefits. Firstly, proliferative cells (red fluorescence) were labelled with Alexa Fluor 594 using Beyo-Click™ EdU cell proliferation kit. The number of EdU-positive cells in the X-ray-treated group was slightly reduced compared to the control group. Conversely, the number of EdU-positive cells was decreased markedly after treatment with IR-83 plus laser irradiation, which was ascribed to the photosensitizing activity of IR-83. Specifically, proliferative cells were rarely observed in cells simultaneously treated with IR-83 plus NIR laser and X-ray irradiation (Fig. 3A). Obviously, the colony formation assay also confirmed that combination with NIR laser irradiation and X-ray plus treatment with IR-83 significantly reduced the number of colonies and inhibited the cell survival fraction of LLC cells (Fig. 3B). To investigate whether combination therapy could alter the radiosensitivity of LLC cells, we also calculated several commonly used parameters that reflected the radio-sensitization effect, including n (extrapolation number), D0 (mean lethal dose), D37 (radiation dose for a survival of 37%), and sensitizer enhancement ratio (SER) values [38]. The values of n, D0, and D37 were 5.327, 1.808, and 4.828, respectively, when treated with X-ray alone, while these values changed to 7.713, 1.164, and 4.828 in the combined group, respectively.

Furthermore, the SER value of "IR-83+ laser irradiation" was 1.33 (Fig. 3C), suggesting that combining the PDT and PTT therapeutic effects of IR-83 with RT enhanced the radio-sensitization of cells rather than just the additive effect of "1 + 1 = 2." Since the SER values of AuNPs and paclitaxel, the two commonly used radiosensitizers, were 1.19 and 1.32, respectively, in lung cancer cells [39,40]. The radio-sensitization effect of IR-83 + laser was comparable to that of AuNPs and paclitaxel.

We next evaluated the synergistic killing effect on LLC cells by detecting the proportion of apoptotic cells. Compared with control group (4.49%), cells treated with X-ray irradiation (4 Gy) (12.46%) or IR-83 followed NIR irradiation (37.14%) exhibited moderate apoptotic effect. In contrast, a significant increase in the apoptotic cell population (62%) was observed in IR-83 plus NIR laser and X-ray irradiation group (Fig. 3D

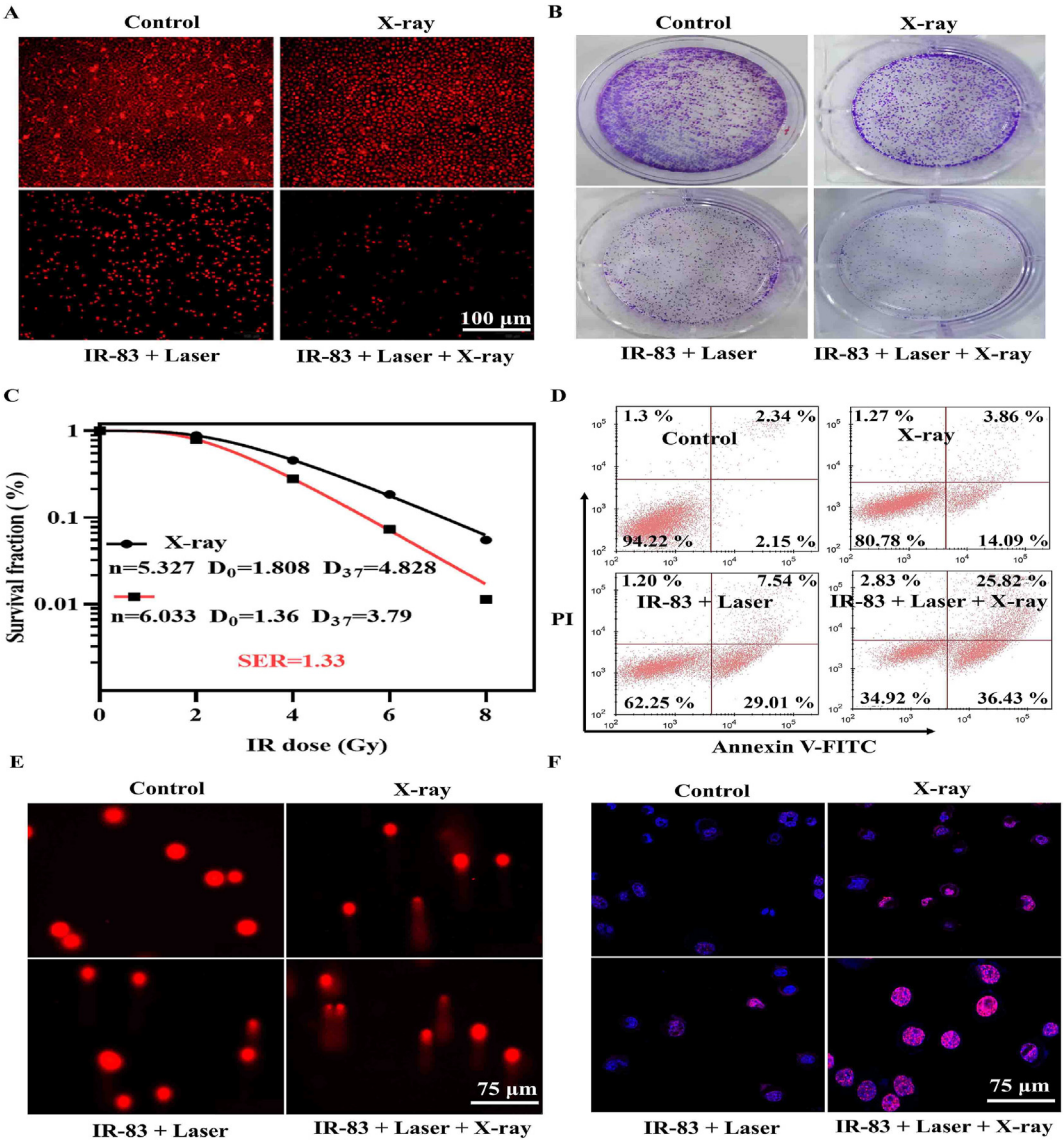

Fig. 3. *In vitro* radio-sensitization effect of IR-83 combined with phototherapy. (A) Fluorescence images of proliferative cells (red) after various treatments. Scale bar: 100 μm. (B) Representative colony formation images of LLC cells after receiving the indicated treatment. (C) Survival fractions of LLC cells in X-ray alone group or IR-83 plus NIR irradiation combined with the X-ray group after exposure to a range of radiation doses (0–8 Gy). (D) Flow cytometric analysis of the cell apoptosis of LLC cells after various treatments. (E) Representative images of comet phenomenon in LLC cells following various treatments. Scale bar: 75 μm. (F) The representative fluorescence images of γ-H2AX staining after various treatments. Blue and pink colors represented DAPI-stained nuclei and γ-H2AX foci, respectively. Scale bar: 75 μm.

and Figure S16A). Western blotting analysis further confirmed that the combination strategy resulted in a prominent increase in the cleavage of caspase-9 and caspase-3 compared with single treatment (Figure S16B-D).

Motivated by the fascinating synergistic killing effect on LLC cells, a neutral comet assay was carried out to confirm the radio-sensitization effect of IR-83-mediated PDT/PTT by quantitating the extent of DSBs. In comparison with control group and "IR-83 + NIR laser" treatment group, X-ray radiation alone resulted in slight comet phenomenon of LLC cells, and the most apparent comet phenomenon can be observed in cells treated with "IR-83 + NIR laser + X-ray" (Fig. 3E). The tail DNA content in combination treatment group was 69%, which is 20 times higher than control group, 14.4 times higher than "IR-83 + NIR laser" group, and 4.4 times than X-ray alone group (Figure S17A). H2AX is a histone variant that is rapidly converted into the phosphorylation form at serine 139 (termed as γ-H2AX) and mediates DNA damage response and DNA repair signaling in response to DSBs. The existing evidence have showed that the occurrence of DSBs can be triggered by exposure to ultraviolet radiation, ionizing radiation, radiomimetic drugs, and ROS [41]. Therefore, γ-H2AX has been widely accepted as a "gold standard" to evaluate the extent of DSBs. As displayed in Fig. 3F and Figure S17B, both the intensity and number of γ-H2AX foci in "IR-83 + NIR laser + X-ray" treatment group were apparently higher than those in any of the three groups, suggesting maximal DNA damage. These results indicated that "IR-83 + laser NIR" could serve as a potential adjuvant strategy to potentiate X-ray irradiation-mediated DNA damage in cells.

2.5. Mitochondria targeting

Existing evidence revealed that mitochondrial biogenesis and quality control are frequently increased in tumour cells and mitochondrial dysfunction could effectively limit tumorigenesis [42]. Mitochondria-targeted therapeutic strategy is gradually considered as a promising method for cancer therapeutic purpose. As a results, numerous mitochondria-specific PS and PTA agent were developed by covalently conjugating with mitochondria-targeting units, such as, triphenylphosphine, rhodamine derivatives, and mitochondria-targeting peptides [43]. Inspired by the fact that cyanine dyes could exhibit excellent mitochondria-targeting capacity owing to its lipophilic and cationic properties, mitochondria targeting characteristic study was thus carried out *in vitro*. We evaluated the mitochondria targeting ability of IR-83 in various cell lines, including LLC, 4T-1, and FRTL5 cells using CLSM following labelling with a commercial Mito-tracker probe. The red fluorescence from IR-83 completely matched the green fluorescence from Mito-tracker to merge as yellow areas in three cell lines, indicating the excellent mitochondria targeting ability of IR-83 (Fig. 4A and Figure S18A). To intuitively visualize the co-localization of IR-83 and mitochondria at the spatial level, we next analyzed the luminescence intensity profiles of red and green fluorescence in the same cells using Image J software. Consistent with the above results, the intensity profiles analysis revealed that the red luminescence signal from IR-83 traced the green fluorescence from mitochondria (Figure S18B). In addition, the average Pearson's correlation coefficient and overlap coefficients in LLC, 4T-1, and FRTL-5 were 0.981/0.979, 0.949/0.970, and 0.949/0.957, respectively (Figure S18C), indicating the high degree (near 100%) overlap of green fluorescence signal (mitochondria-tracker) and red fluorescence signal (IR-83 dyes). The Pearson's colocalization coefficient of IR-83 is apparently higher than some mitochondria targetable fluorescent probes that reported in published literature [36,44]. These data validate IR-83 was efficiently internalized into tumour cells and specifically accumulated in mitochondria.

2.6. IR-83 acts as a "mito-bomb" and controls mitochondrial network

By virtue of the excellent mitochondria targeting and dual-modal PDT and PTT therapeutic capabilities of IR-83, we speculated that IR-83 might serve as a specific mitochondria "bomb" under NIR/X-ray local irradiation, leading to mitochondria dysfunction owing to hyperthermia effect and ROS burst. It's well accepted that mitochondrial are extensively dynamic organelles and the number, shape, and size of mitochondria were tightly controlled by the net balance between mitochondrial fusion and fission [45]. Such as, a reduction in fission or increase in fusion might lead to the formation of bigger, little number mitochondria. As shown in Fig. 4B and Figure S19A, no obvious difference in the size, number, shape of mitochondrial between control group and X-ray group were found. In contrast, "IR-83 + NIR laser" treatment results in a decrease of mitochondrial number, as well as an increase of mitochondrial size. In addition, a notably increase of mitochondria fragmentation were observed in cells treated with IR-83 upon both X-ray and NIR irradiation, when compared with X-ray irradiation or IR-83 + NIR laser group. The term of "mitochondrial network" refers to the separate, punctate individual mitochondria, as well as the branched, reticular structure of fused mitochondria in eukaryotic cell [46]. We therefore analyzed the mitochondrial network using Mitochondrial Network Analysis toolset and several network parameters were calculated. As compared to control and X-ray group, IR-83-mediated PDT and PTT induced by NIR irradiation obviously increased the number of individuals (puncta and rods) (2.6 folds and 3.1 folds for control and X-ray group, respectively) and networks (2.1 folds and 2.2 folds for control and X-ray group, respectively). Moreover, the combination group showed fewest number of individuals and networks due to abundant existence of mitochondria fragmentation (Figure S19B-C). The combined treatment also resulted in the decrease in number of branches per network (Figure S19D), which was related to the fragmentation of larger networks with more branches into many smaller networks when mitochondria fragmentation occurs. In another respect, mitochondrial footprint was also obviously decreased following by "IR-83 + NIR laser + X-ray" treatment (Figure S19E), perhaps owing to the mitophagy of the fragmented mitochondria [47]. Consistently, TEM imaging displayed that the combined strategy induced mitochondria fragmentation, swelling, crista disorder, and increased electron density (Fig. 4C). These data clearly revealed that IR-83-mediated PDT and PTT could resulted in mitochondria morphological and structural alterations.

Our aforementioned findings suggested that combined treatment strategy can obviously alter mitochondrial morphology and size, we therefore speculated the function of mitochondria might be profoundly affected. To verify our consumption, JC-1 staining was carried out to determine the alteration of mitochondrial membrane potential (MMP), which is essential to maintain the mitochondrial function [48]. Compared to the control, an obvious increase in green fluorescence (JC-1 monomer refers to loss of membrane potential) was observed in the IR-83 plus NIR laser group, while fluorescence intensity had no significant alteration in the irradiation alone group. Similarly, the combined group exhibited the maximal increase in green fluorescence signal and decrease in red fluorescence signal (JC-1 aggregates refer to high membrane potential) than that of the other groups, indicating that the loss of MMP that was induced by "IR-83 + NIR laser" was enhanced with the participation of X-ray irradiation (Figure S20A-B). The significant loss of MMP might subsequently contributed to the activation of the mitochondrial apoptotic pathway. On the other aspect, mitochondria are the vital organelles for cell survival as they are central hubs for energy production and ATP generation (>90%) via OXPHOS pathway [49]. Mitochondrial OXPHOS has been proved to promote cancer cell resistance to radiotherapy and chemotherapy [50,51]. Thus, it is speculated that inhibition of mitochondrial OXPHOS can reduce fuel supply and decrease O_2 consumption, which may improve sensitivity and restrain tumour cell metastasis [52]. The production of ATP in IR-83 + NIR laser-treated cells was significantly lower than that in the PBS or X-ray treatment groups. Notably, the cells treated with IR-83 plus NIR laser and X-ray irradiation showed the lowest ATP level than that in any other treatments (Figure S20C). The results indicated that "IR-83 + NIR laser + X-ray" could effectively inhibit mitochondrial OXPHOS process, reduce cellular ATP generation, and decrease O_2 consumption to sensitize radiotherapy.

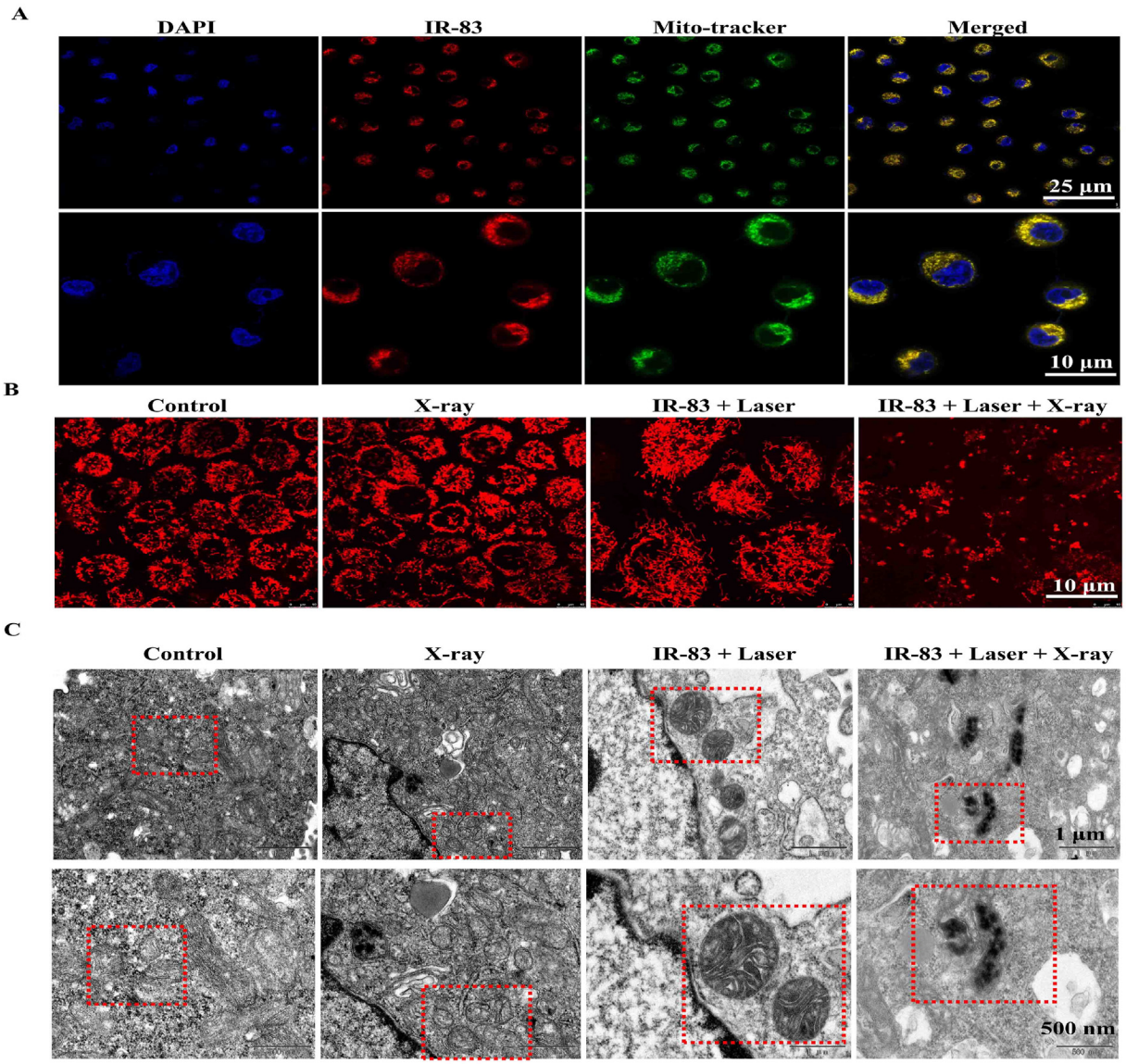

Fig. 4. Effect of combined treatment on mitochondria morphology and function. (A) Confocal fluorescence images of LLC cells incubated with IR-83 (2.5 μM) for 4 h. Blue, green, and red colors represent DAPI-stained cell nuclei, Mitotracker, and IR-83 fluorescence, respectively. (B) CLSM images of mitochondria morphology in each group after labelling with mitochondria-specific probe (red). (C) TEM images of mitochondria in LLC cells after various treatments.

2.7. Dysfunction of antioxidant defense system

Considering that mitochondria are the prominent sources of cellular ROS generation (>90%) and oxidation stress balance, a commercial ROS detection probe (DCFH-DA) was employed to detect the generation of ROS [53]. As shown in Fig. 5A, LLC cells treated with IR-83 plus NIR laser showed increased fluorescence intensity than that in control group or X-ray alone group. Interestingly, maximal amount of ROS was generated in cells treated with "IR-83 + NIR laser + X-ray". Some previous reports have revealed that RT efficacy could be effectively improved through inducing mitochondrial ROS burst [42,54]. Furthermore, excessive ROS also could cause damage to mitochondrial DNA, which subsequently reduces the synthesis of ATP, decreases MMP, and increases the release of Cyt *c*. Consistently, the current results showed that the synergistic effect on ROS generation might contribute to the radiotherapy sensitization effect of IR-83 and it improved the efficacy of RT in a ROS-dependent manner. Excessive ROS (oxidative stress) directly results in biomolecular damage and programmed cell death, disrupting mitochondrial integrity. In physiological conditions, ROS levels are controlled by intracellular antioxidant systems, such as reduced forms of glutathione (GSH), nuclear factor erythroid-derived 2-like 2 (Nrf2), and heme oxygenase 1 (HO-1) [55]. IR-83 plus NIR irradiation and X-ray resulted in obvious GSH and nicotinamide adenine dinucleotide phosphate (NADPH) depletion compare to other groups (Fig. 5B and C), indicating the decreased of anti-oxidative capability. Nrf2 has been proved to maintain mitochondrial redox homeostasis through generating GSH, NADPH, and several mitochondrial antioxidant enzymes, such as HO-1 [56]. It's worth noting that the protein expression levels of Nrf2 and HO-1 were extraordinarily increased in LLC cells treated with "IR-83 + NIR laser" when compared with control group or X-ray group, which might be explained by the ROS stress response of tumour cells. Conversely, a sharp decrease of Nrf2 and HO-1 level were observed in cells subject to the treatment strategy of "IR-83+ NIR laser + X-ray", thanks to the synergetic effect on ROS generation and mitochondrial dysfunction (Fig. 5D and E). Collectively, the numerous ROS generation induced by "IR-83+ NIR laser + X-ray" might be explained by two aspects: (1) The synergistic effect of IR-83-mediated PDT and X-ray on ROS production; (2) The dysfunction of antioxidant defense systems, which leads to the reduction of scavenging capacities of ROS. These findings indicated that the combination treatment alleviated Nrf2-mediated

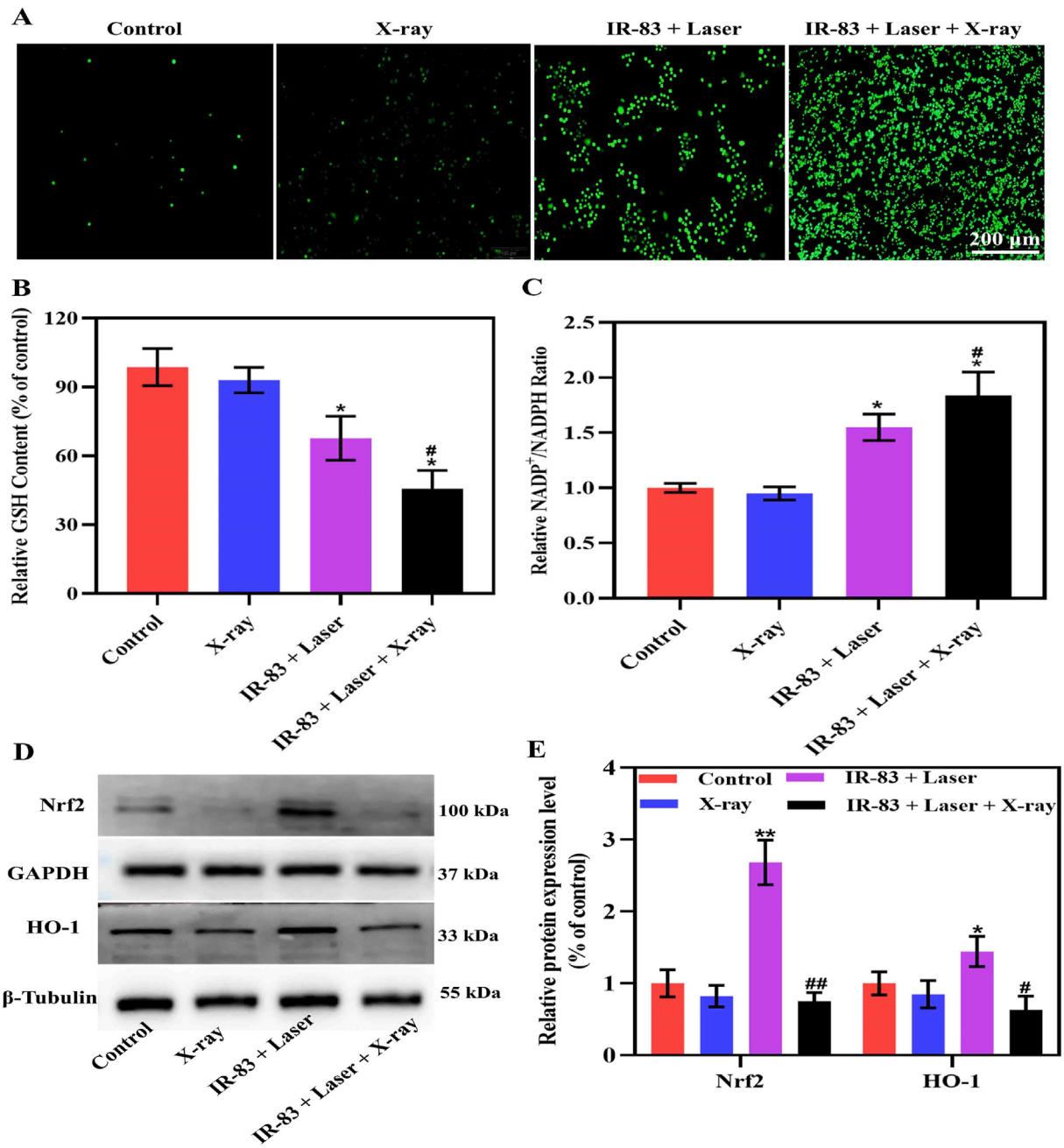

Fig. 5. Effect of combined treatment on Nrf2-mediated antioxidant system. (A) Generation of ROS in LLC cells after different treatments as indicated determined by DCFH-DA staining under the confocal microscope. (B) Relative GSH level and $NADP^+$/NADPH ratio C) in LLC cells after receiving various treatments as indicated. (D) Western blotting analysis of Nrf2 and HO-1 protein expression in LLC cells after receiving various treatments for 24 h. (E) Semi-quantification expression levels of Nrf2 and HO-1 in cells. GAPDH and β-tubulin were selected as internal controls for Nrf2 and HO-1, respectively. "*" Significantly different from control group; "#" Significantly different from X-ray alone group; *P < 0.05, **P < 0.01, #P < 0.05, ##P < 0.01.

antioxidant and detoxification in tumour cells, which in turn improved therapeutic efficacy against tumour cells.

2.8. Synergistic effect on metastasis and angiogenesis

Metastasis causes most of cancer-related mortality and yet remains one of the principal obstacles for successful tumour elimination [57]. Since tumour vessels act as transfer channels in tumour metastasis that allow cancer cells to escape the primary lesion and disseminate into surrounding structures or distant sites [58]. Thus, targeting angiogenesis represents an effective approach to limit tumour cell invasiveness and increase the efficacy of tumour therapy. Next, we investigated whether the combination treatment of IR-83-mediated phototherapy and X-ray irradiation could suppress tumour metastasis and angiogenesis *in vitro*. We found that cells in the combined group exhibited the strongest inhibitory effects on migratory and invasive activities compared to the cells subjected to other treatments (Figure S21). Mild hyperthermia increased the permeability of the tumour vessels, while extreme hyperthermia disrupted tumour vasculature by interfering with the proliferation and migration of endothelial cells [59]. As anticipated, tube formation assay results confirmed that low dose X-ray irradiation caused a negligible effect on angiogenesis compared to the control. Conversely, the combination of IR-83 and laser irradiation plus X-ray resulted in fewer tube formations, as evidenced by the reduced vessels density and

vessels length, which might be attributed to the hyperthermia effect of IR-83 (Figure S22). The aforementioned findings demonstrated that the combined strategy suppresses cell migration, invasiveness and angiogenesis *in vitro*.

2.9. In vivo RT/PDT/PTT synergistic anti-tumour activity

The robust synergistic effect of IR-83 with RT *in vitro* motivated us to further investigate its therapeutic efficiency *in vivo*. A volume of 100 μL IR-83 (2.5 mg/kg in PBS) or PBS was administered to LLC tumour-bearing mice via intravenous tail injection when the volume reached experimental requirements (~100 mm^3) (day 9). After 24 h, the tumour sites were exposed to 808 nm NIR laser irradiation for 5 min at the power density of 0.8 W/cm^2. Then, 5 min after laser irradiation, mice were subjected to X-ray irradiation at a single dose of 6 Gy. The tumour volume and body weight were recorded every 3 days, and the animals were sacrificed at day 21 (Fig. 6A). As reflected in Fig. 6C, compared to the vehicle control group, X-ray irradiation treatment group exhibited a slight tumour suppression tendency. Moreover, IR-83 plus laser irradiation showed a much better therapeutic effect on tumour growth inhibition, which in turn demonstrated excellent phototherapeutic effect of IR-83 on killing cancer cells. Consistent with the *in vitro* results, the combined group exhibited the best antitumor efficacy compared with single treatment groups. The tumour tissues images and tumour weight data further validated that although both X-ray irradiation or IR-83 plus laser irradiation alleviated tumour growth to some extent, integrating the two therapeutic regimens substantially minimized the tumour tissues that even disappeared completely (Fig. 6B). No obvious difference was detected in the mice body weight among the all groups (Figure S23A), suggesting that this compound did not cause severe systemic toxicity. The tumour sections were further subjected to Ki-67 and TUNEL immunochemical staining. Results showed that IR-83 plus laser irradiation and subsequent ionizing radiation led to the maximal decrease of Ki-67-postive cells (Figure S23B-C) and increase of TUNEL-positive cells (Figure S24). Meanwhile, the expression levels of cleaved caspase-9 and cleaved caspase-3 also showed the similar trend (Figure S25). Additionally, the mice in IR-83 plus laser irradiation plus IR treated group achieved longer survival time (>45 days) than those receiving other

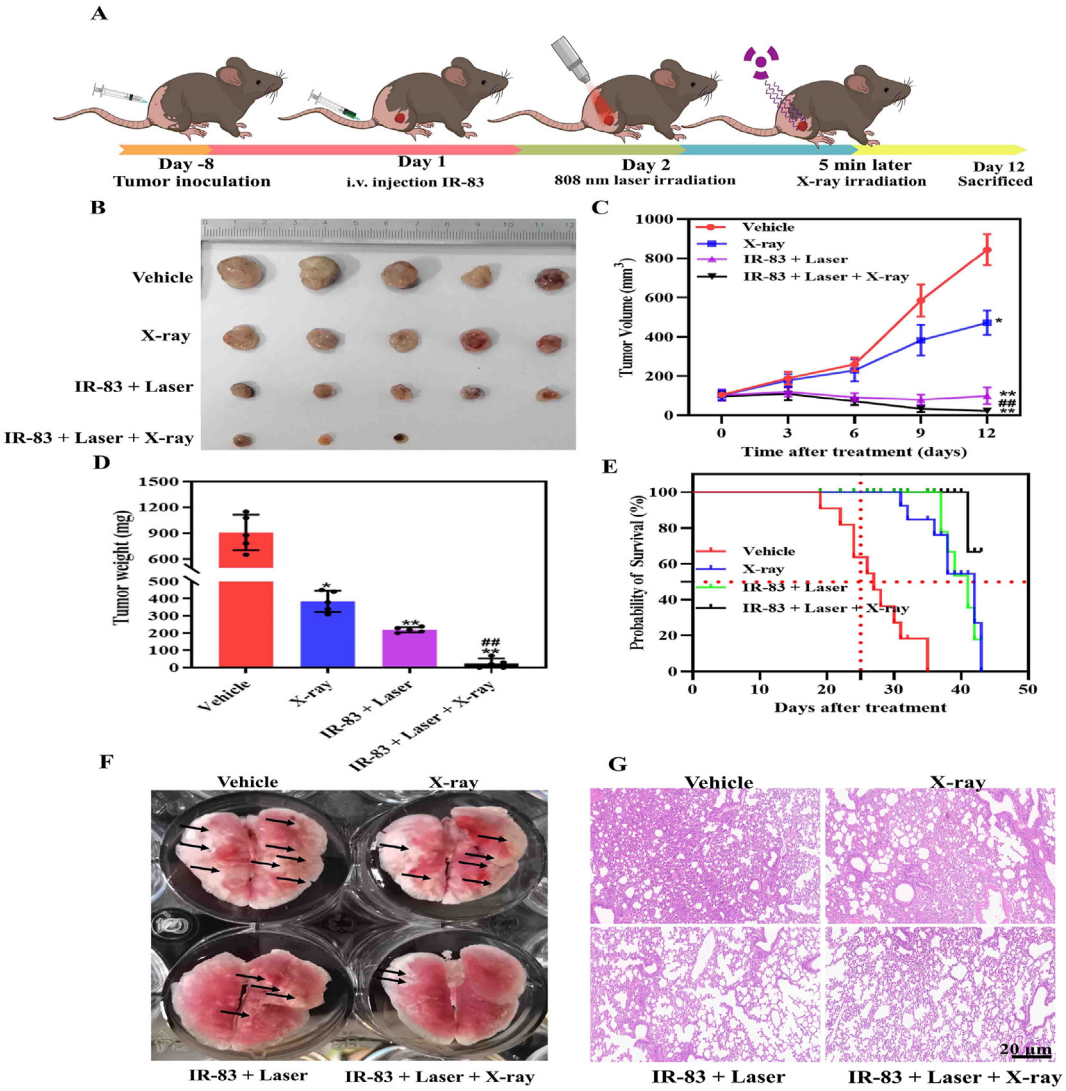

Fig. 6. Anti-tumour activity of combined treatment *in vivo*. (A) Schematic illustration of the schedule for antitumor studies in LLC tumour-bearing mice. (B) Photographs of tumour tissues dissected from each group on day 21. (C) Tumour volume curves of different groups of mice after receiving the indicated treatments in 12 days (n = 5 per group). (D) Tumour weight of mice over 12 days after different treatments (n = 5 per group). (E) Probability of free survival of tumour-bearing mice in each group after receiving various treatments as indicated. (F) Representative images of lung tissues collected from different groups of mice. Black arrow indicated lung metastasis nodes. (G) Representative micrographs of H&E-stained lung sections were collected from different groups of mice. Scale bar: 20 μm. Error bars represent mean ± S.D. "*" Significantly different from vehicle group; "#" Significantly different from X-ray alone group; *P < 0.05, **P < 0.01, ##P < 0.01.

treatments (20–35 days) (Fig. 6E). These findings corroborated with the previous findings showed that PTT and PDT could serve as potential adjuvant therapy for RT in practical application.

Lung is recognized as the most frequent site of metastasis for various malignancies, including lung cancer and breast cancer. Hence, we also examined lung metastases by directly observing the metastatic node using hematoxylin and eosin (H&E) pathological staining. As displayed in Fig. 6F and G, visible pulmonary metastasis nodes were observed in the lung of control animals, whereas no obvious influence was detected on lung metastases upon exposure to low-dose *X*-ray. Markedly, the number of metastatic lesions in IR-83 plus laser group decreased, and the combined treatment exhibited negligible tumour nodules, which was attributed to the phototherapeutic effect of IR-83. Consistent with *in vitro* observation, immunohistochemistry analysis revealed that reduced CD34 expression, a frequently used specific marker for vascular endothelial cells [60] was obviously found in combined group (Supplementary Fig. 19). Consecutively, the expression levels of HIF-1α and VEGF, critical mediators of angiogenesis and carcinogenesis [61], especially for hypoxic solid tumours, were obviously down-regulated in the combined group compared to the other groups (Figure S26). The reduced HIF-1α/VEGF expression might be responsible for the inhibitory effect on tumour angiogenesis. Collectively, these findings suggested that the combined strategy exhibited a synergistic inhibitory effect on tumour metastasis and angiogenesis. Based on these results, we concluded that the combination strategy was effective in inhibiting cell migration and invasiveness. Isobologram analysis is a widely accepted methods to classify the combined effects (antagonistic, additive, and synergistic effect) of two or more treatment modalities [62], which prompted us to investigate the interaction between the phototherapy of IR-83 and RT *in vitro*. The isobologram analysis revealed that the combination strategy exerts a synergistic killing effect on LLC cells and tumour growth, supported by the fact that the combined point was below the line defining the additive effects (Figure S27). In summary, these findings indicated that "IR-83 + laser" improved the radiosensitivity of cancer cells to ionizing radiation, yielding a supra-additive synergistic effect of "$1 + 1 > 2$". Finally, the body weight, liver/kidney function, and blood routine index were tested during the various treatments to evaluate the biosafety of IR-83. H&E staining was performed to examine the histological changes in the viscera (heart, liver, spleen, and kidney). The mice treated with IR-83 did not exhibit any obvious organ damage and inflammatory lesions compared to the controls (Figure S28). The blood biochemical analysis (CREA, UREA, ALT, and AST) (Figure S29) and hematological parameters (WBC, RBC, and PLT) (Figure S30) among groups did not show obvious abnormality. These results suggested that the tumour-targeting multimodal treatment might designate IR-83 as an excellent anticancer agent without perceptible side effects.

3. Conclusion

As Paul Ehrlich [63] mentioned, a therapeutic drug molecule likes a "magic bullet" should go straight to its cell receptor target. In view of this, an ideal dual-targeted phototherapeutic agent for cancer should possess three levels of specific selectivity, namely tumour area accumulation, tumour cell targeting, intracellular organelles targeting. Taken together, we developed a multifunctional NIR fluorophore (IR-83) for hypoxic tumour-targeted RT/PDT/PTT triple synergistic therapy. IR-83 was synthesized by introducing a hypoxia-targeting ligand, 2-nitroimidazole, into the framework of heptamethine cyanine dyes. Firstly, IR-83 selectively accumulated in the tumour region and identified the tumours and adjacent boundaries owing to its excellent tumour-targeting and NIR imaging capabilities. Secondly, IR-83 suppressed tumour growth, metastasis, and angiogenesis by synchronously integrating radio/-photodynamic/photothermal multimodal therapies. Finally, IR-83 was specifically anchored in cancer cell mitochondria, causing mitochondrial dysfunction upon exposure to NIR laser, which in turn led to antioxidant defense system imbalance, OXPHOS inhibition, a decline in O_2 consumption and programmed cell death. The current study established an effective strategy to improve the efficacy of RT against cancer by integrating mitochondria-targeted small molecular-mediated PDT and PTT effects.

Funding

This work was supported by the National Natural Science Foundation of China (grant number: 82173457), Chongqing Youth Talent Project (grant number: cstc2021ycjh-bgzxm0123), Outstanding Youth Development Program in Third Military Medical University (No. 2017), Intramural Research Project Grant (AEP17J001), and Technology Innovation and R&D Projects of Chengdu Science and Technology Bureau (2021-YF05-01659-SN).

Credit author statement

Mingquan Gao: Methodology, Investigation, Formal analysis, Data curation, Writing-original draft. **Xie Huang**: Methodology, Validation, Formal analysis. **Zifei Wu**: Formal analysis. **Liting Wang**: Methodology, Resources. **Shaolong Yuan**: Formal analysis. **Zaizhi Du**: Data curation, Investigation. **Shenglin Luo**: Conceptualization Methodology, Investigation, Funding acquisition. **Rong Li**: Conceptualization, Supervision, Project administration, Writing re-view & editing. **Weidong Wang**: Conceptualization, Supervision, Funding acquisition, Writing re-view & editing.

Declaration of competing interest

The authors declare that they have no known competing financial interests or personal relationships that could have appeared to influence the work reported in this paper.

Appendix A. Supplementary data

Supplementary data to this article can be found online at https://doi.org/10.1016/j.mtbio.2022.100316.

References

[1] E.C. Ko, D. Raben, S.C. Formenti, The integration of radiotherapy with immunotherapy for the treatment of non-small cell lung cancer, Clin. Cancer Res. 24 (23) (2018) 5792–5806.
[2] W.L. Santivasi, F. Xia, Ionizing radiation-induced DNA damage, response, and repair, Antioxidants Redox Signal. 21 (2) (2014) 251–259.
[3] A. Noda, Y. Hirai, K. Hamasaki, H. Mitani, N. Nakamura, Y. Kodama, Unrepairable DNA double-strand breaks that are generated by ionising radiation determine the fate of normal human cells, J. Cell Sci. 125 (Pt 22) (2012) 5280–5287.
[4] M.R. Horsman, J. Overgaard, The impact of hypoxia and its modification of the outcome of radiotherapy, J. Radiat. Res. 57 (Suppl 1) (2016) i90–i98. Suppl 1.
[5] C.Y. Yu, H. Xu, S. Ji, R.T. Kwok, J.W. Lam, X. Li, S. Krishnan, D. Ding, B.Z. Tang, Mitochondrion-anchoring photosensitizer with aggregation-induced emission characteristics synergistically boosts the radiosensitivity of cancer cells to ionizing radiation, Adv. Mater. 29 (15) (2017).
[6] K. Ni, G. Lan, S.S. Veroneau, X. Duan, Y. Song, W. Lin, Nanoscale metal-organic frameworks for mitochondria-targeted radiotherapy-radiodynamic therapy, Nat. Commun. 9 (1) (2018) 4321.
[7] T.I. Liu, T.Y. Lu, Y.C. Yang, S.H. Chang, H.H. Chen, I.L. Lu, A. Sabu, H.C. Chiu, New combination treatment from ROS-Induced sensitized radiotherapy with nanophototherapeutics to fully eradicate orthotopic breast cancer and inhibit metastasis, Biomaterials 257 (2020), 120229.
[8] X. Li, J.F. Lovell, J. Yoon, X. Chen, Clinical development and potential of photothermal and photodynamic therapies for cancer, Nat. Rev. Clin. Oncol. 17 (11) (2020) 657–674.
[9] D. Chen, Q. Xu, W. Wang, J. Shao, W. Huang, X. Dong, Type I Photosensitizers Revitalizing Photodynamic Oncotherapy, Small, Weinheim an der Bergstrasse, Germany), 2021, e2006742.
[10] Q. Wang, N. Liu, Z. Hou, J. Shi, X. Su, X. Sun, Radioiodinated persistent luminescence nanoplatform for radiation-induced photodynamic therapy and radiotherapy, Adv. Healthcare Mater. 10 (5) (2021), e2000802.
[11] B.S. Dash, S. Das, J.P. Chen, Photosensitizer-functionalized nanocomposites for light-activated cancer theranostics, Int. J. Mol. Sci. 22 (13) (2021).
[12] D. Zhi, T. Yang, J. O'Hagan, S. Zhang, R.F. Donnelly, Photothermal therapy, J. Contr. Release 325 (2020) 52–71.

[13] K. Yang, S. Zhang, G. Zhang, X. Sun, S.T. Lee, Z. Liu, Graphene in mice: ultrahigh in vivo tumor uptake and efficient photothermal therapy, Nano Lett. 10 (9) (2010) 3318–3323.
[14] C.W. Song, M.S. Kang, J.G. Rhee, S.H. Levitt, The effect of hyperthermia on vascular function, pH, and cell survival, Radiology 137 (3) (1980) 795–803.
[15] M. Dunne, M. Regenold, C. Allen, Hyperthermia can alter tumor physiology and improve chemo- and radio-therapy efficacy, Adv. Drug Deliv. Rev. 163–164 (2020) 98–124.
[16] M.R. Horsman, Tissue physiology and the response to heat, Int. J. Hyperther. 22 (3) (2006) 197–203.
[17] N.R. Datta, E. Puric, D. Klingbiel, S. Gomez, S. Bodis, Hyperthermia and radiation therapy in locoregional recurrent breast cancers: a systematic review and meta-analysis, Int. J. Radiat. Oncol. Biol. Phys. 94 (5) (2016) 1073–1087.
[18] N.R. Datta, S. Rogers, D. Klingbiel, S. Gómez, E. Puric, S. Bodis, Hyperthermia and radiotherapy with or without chemotherapy in locally advanced cervical cancer: a systematic review with conventional and network meta-analyses, Int. J. Hyperther. 32 (7) (2016) 809–821.
[19] C. Song, W. Xu, Z. Wei, C. Ou, J. Wu, J. Tong, Y. Cai, X. Dong, W. Han, Anti-LDLR modified TPZ@Ce6-PEG complexes for tumor hypoxia-targeting chemo-/radio-/photodynamic/photothermal therapy, J. Mater. Chem. B 8 (4) (2020) 648–654.
[20] Z. Guo, S. Zhu, Y. Yong, X. Zhang, X. Dong, J. Du, J. Xie, Q. Wang, Z. Gu, Y. Zhao, Synthesis of BSA-coated BiOI@Bi(2) S(3) semiconductor heterojunction nanoparticles and their applications for radio/photodynamic/photothermal synergistic therapy of tumor, Adv. Mater. 29 (44) (2017).
[21] X. Xu, Y. Chong, X. Liu, H. Fu, C. Yu, J. Huang, Z. Zhang, Multifunctional nanotheranostic gold nanocages for photoacoustic imaging guided radio/photodynamic/photothermal synergistic therapy, Acta Biomater. 84 (2019) 328–338.
[22] Z.X. Zhao, Y.Z. Huang, S.G. Shi, S.H. Tang, D.H. Li, X.L. Chen, Cancer therapy improvement with mesoporous silica nanoparticles combining photodynamic and photothermal therapy, Nanotechnology 25 (28) (2014), 285701.
[23] P. Agostinis, K. Berg, K.A. Cengel, T.H. Foster, A.W. Girotti, S.O. Gollnick, S.M. Hahn, M.R. Hamblin, A. Juzeniene, D. Kessel, M. Korbelik, J. Moan, P. Mroz, D. Nowis, J. Piette, B.C. Wilson, J. Golab, Photodynamic therapy of cancer: an update, CA Cancer J. Clin. 61 (4) (2011) 250–281.
[24] J. Schuemann, R. Berbeco, D.B. Chithrani, S.H. Cho, R. Kumar, S.J. McMahon, S. Sridhar, S. Krishnan, Roadmap to clinical use of gold nanoparticles for radiation sensitization, Int. J. Radiat. Oncol. Biol. Phys. 94 (1) (2016) 189–205.
[25] S. Luo, X. Tan, Q. Qi, Q. Guo, X. Ran, L. Zhang, E. Zhang, Y. Liang, L. Weng, H. Zheng, T. Cheng, Y. Su, C. Shi, A multifunctional heptamethine near-infrared dye for cancer theranosis, Biomaterials 34 (9) (2013) 2244–2251.
[26] X. Tan, S. Luo, D. Wang, Y. Su, T. Cheng, C. Shi, A NIR heptamethine dye with intrinsic cancer targeting, imaging and photosensitizing properties, Biomaterials 33 (7) (2012) 2230–2239.
[27] S. Luo, X. Tan, S. Fang, Y. Wang, T. Liu, X. Wang, Y. Yuan, H. Sun, Q. Qi, C. Shi, Mitochondria-targeted small-molecule fluorophores for dual modal cancer phototherapy, Adv. Funct. Mater. 26 (17) (2016) 2826–2835.
[28] X. Tan, S. Luo, L. Long, Y. Wang, D. Wang, S. Fang, Q. Ouyang, Y. Su, T. Cheng, C. Shi, Structure-guided design and synthesis of a mitochondria-targeting near-infrared fluorophore with multimodal therapeutic activities, Adv. Mater. (Deerfield Beach, Fla.) 29 (43) (2017).
[29] S. Chen, S. Yu, Z. Du, X. Huang, M. He, S. Long, J. Liu, Y. Lan, D. Yang, H. Wang, S. Li, A. Chen, Y. Hao, Y. Su, C. Wang, S. Luo, Synthesis of mitochondria-anchored nitroimidazoles with a versatile NIR fluorophore for hypoxic tumor-targeting imaging and chemoradiotherapy, J. Med. Chem. 64 (6) (2021) 3381–3391.
[30] Y. Long, J. Liu, D. Tian, F. Dai, S. Zhang, B. Zhou, Cooperation of ESIPT and ICT processes in the designed 2-(2'-hydroxyphenyl)benzothiazole derivative: a near-infrared two-photon fluorescent probe with a large Stokes shift for the detection of cysteine and its application in biological environments, Anal. Chem. 92 (20) (2020) 14236–14243.
[31] Y. Huang, C. Jin, J. Yu, L. Wang, W. Lu, A novel multifunctional 2-nitroimidazole-based bioreductive linker and its application in hypoxia-activated prodrugs, Bioorg. Chem. 101 (2020), 103975.
[32] S. Bharathiraja, P. Manivasagan, M. Santha Moorthy, N.Q. Bui, B. Jang, T.T.V. Phan, W.K. Jung, Y.M. Kim, K.D. Lee, J. Oh, Photo-based PDT/PTT dual model killing and imaging of cancer cells using phycocyanin-polypyrrole nanoparticles, Eur. J. Pharm. Biopharm. 123 (2018) 20–30.
[33] N. Yu, Z. Wang, J. Zhang, Z. Liu, B. Zhu, J. Yu, M. Zhu, C. Peng, Z. Chen, Thiol-capped Bi nanoparticles as stable and all-in-one type theranostic nanoagents for tumor imaging and thermoradiotherapy, Biomaterials 161 (2018) 279–291.
[34] C.M. Hessel, V.P. Pattani, M. Rasch, M.G. Panthani, B. Koo, J.W. Tunnell, B.A. Korgel, Copper selenide nanocrystals for photothermal therapy, Nano Lett. 11 (6) (2011) 2560–2566.
[35] Q. Tian, F. Jiang, R. Zou, Q. Liu, Z. Chen, M. Zhu, S. Yang, J. Wang, J. Wang, J. Hu, Hydrophilic Cu9S5 nanocrystals: a photothermal agent with a 25.7% heat conversion efficiency for photothermal ablation of cancer cells in vivo, ACS Nano 5 (12) (2011) 9761–9771.
[36] R. Guo, H. Peng, Y. Tian, S. Shen, W. Yang, Mitochondria-targeting magnetic composite nanoparticles for enhanced phototherapy of cancer, Small 12 (33) (2016) 4541–4552.
[37] X. Cheng, Y. Yong, Y. Dai, X. Song, G. Yang, Y. Pan, C. Ge, Enhanced radiotherapy using bismuth sulfide nanoagents combined with photo-thermal treatment, Theranostics 7 (17) (2017) 4087–4098.
[38] H.D. Thames, H.D. Suit, Tumor radioresponsiveness versus fractionation sensitivity, Int. J. Radiat. Oncol. Biol. Phys. 12 (4) (1986) 687–691.
[39] T. Kuhnt, A. Becker, M. Bloching, J. Schubert, G. Klautke, R. Fietkau, J. Dunst, Phase II trial of a simultaneous radiochemotherapy with cisplatinum and paclitaxel in combination with hyperfractionated-accelerated radiotherapy in locally advanced head and neck tumors, Med. Oncol. 23 (3) (2006) 325–333.
[40] X.D. Zhang, D. Wu, X. Shen, J. Chen, Y.M. Sun, P.X. Liu, X.J. Liang, Size-dependent radiosensitization of PEG-coated gold nanoparticles for cancer radiation therapy, Biomaterials 33 (27) (2012) 6408–6419.
[41] D. Chowdhury, X. Xu, X. Zhong, F. Ahmed, J. Zhong, J. Liao, D.M. Dykxhoorn, D.M. Weinstock, G.P. Pfeifer, J. Lieberman, A PP4-phosphatase complex dephosphorylates gamma-H2AX generated during DNA replication, Mol. Cell 31 (1) (2008) 33–46.
[42] Z. Yu, Q. Sun, W. Pan, N. Li, B. Tang, A near-infrared triggered nanophotosensitizer inducing domino effect on mitochondrial reactive oxygen species burst for cancer therapy, ACS Nano 9 (11) (2015) 11064–11074.
[43] X. Guo, N. Yang, W. Ji, H. Zhang, X. Dong, Z. Zhou, L. Li, H.M. Shen, S.Q. Yao, W. Huang, Mito-bomb: targeting mitochondria for cancer therapy, Adv. Mater. 33 (43) (2021), e2007778.
[44] H. Yu, X. Zhang, Y. Xiao, W. Zou, L. Wang, L. Jin, Targetable fluorescent probe for monitoring exogenous and endogenous NO in mitochondria of living cells, Anal. Chem. 85 (15) (2013) 7076–7084.
[45] D.C. Chan, Mitochondrial dynamics and its involvement in disease, Annu. Rev. Pathol. 15 (2020) 235–259.
[46] L.L. Xie, F. Shi, Z. Tan, Y. Li, A.M. Bode, Y. Cao, Mitochondrial network structure homeostasis and cell death, Cancer Sci. 109 (12) (2018) 3686–3694.
[47] G. Twig, A. Elorza, A.J. Molina, H. Mohamed, J.D. Wikstrom, G. Walzer, L. Stiles, S.E. Haigh, S. Katz, G. Las, J. Alroy, M. Wu, B.F. Py, J. Yuan, J.T. Deeney, B.E. Corkey, O.S. Shirihai, Fission and selective fusion govern mitochondrial segregation and elimination by autophagy, EMBO J. 27 (2) (2008) 433–446.
[48] A. Perelman, C. Wachtel, M. Cohen, S. Haupt, H. Shapiro, A. Tzur, JC-1: alternative excitation wavelengths facilitate mitochondrial membrane potential cytometry, Cell Death Dis. 3 (11) (2012), e430.
[49] D. Nolfi-Donegan, A. Braganza, S. Shiva, Mitochondrial electron transport chain: oxidative phosphorylation, oxidant production, and methods of measurement, Redox Biol. 37 (2020), 101674.
[50] C.T. Hensley, B. Faubert, Q. Yuan, N. Lev-Cohain, E. Jin, J. Kim, L. Jiang, B. Ko, R. Skelton, L. Loudat, M. Wodzak, C. Klimko, E. McMillan, Y. Butt, M. Ni, D. Oliver, J. Torrealba, C.R. Malloy, K. Kernstine, R.E. Lenkinski, R.J. DeBerardinis, Metabolic heterogeneity in human lung tumors, Cell 164 (4) (2016) 681–694.
[51] A. Viale, D. Corti, G.F. Draetta, Tumors and mitochondrial respiration: a neglected connection, Cancer Res. 75 (18) (2015) 3685–3686.
[52] P. Ghosh, C. Vidal, S. Dey, L. Zhang, Mitochondria targeting as an effective strategy for cancer therapy, Int. J. Mol. Sci. 21 (9) (2020).
[53] E. Eruslanov, S. Kusmartsev, Identification of ROS using oxidized DCFDA and flow-cytometry, Methods Mol. Biol. 594 (2010) 57–72.
[54] N. Li, L. Yu, J. Wang, X. Gao, Y. Chen, W. Pan, B. Tang, A mitochondria-targeted nanoradiosensitizer activating reactive oxygen species burst for enhanced radiation therapy, Chem. Sci. 9 (12) (2018) 3159–3164.
[55] G.M. DeNicola, F.A. Karreth, T.J. Humpton, A. Gopinathan, C. Wei, K. Frese, D. Mangal, K.H. Yu, C.J. Yeo, E.S. Calhoun, F. Scrimieri, J.M. Winter, R.H. Hruban, C. Iacobuzio-Donahue, S.E. Kern, I.A. Blair, D.A. Tuveson, Oncogene-induced Nrf2 transcription promotes ROS detoxification and tumorigenesis, Nature 475 (7354) (2011) 106–109.
[56] I.G. Ryoo, M.K. Kwak, Regulatory crosstalk between the oxidative stress-related transcription factor Nfe2l2/Nrf2 and mitochondria, Toxicol. Appl. Pharmacol. 359 (2018) 24–33.
[57] C.L. Chaffer, R.A. Weinberg, A perspective on cancer cell metastasis, Science 331 (6024) (2011) 1559–1564.
[58] L. Schito, Hypoxia-dependent angiogenesis and lymphangiogenesis in cancer, Adv. Exp. Med. Biol. 1136 (2019) 71–85.
[59] D.L. Liu, S. Andersson-Engels, C. Sturesson, K. Svanberg, C.H. Håkansson, S. Svanberg, Tumour vessel damage resulting from laser-induced hyperthermia alone and in combination with photodynamic therapy, Cancer Lett. 111 (1–2) (1997) 157–165.
[60] M. Murga, L. Yao, G. Tosato, Derivation of endothelial cells from CD34- umbilical cord blood, Stem Cell. 22 (3) (2004) 385–395.
[61] G.N. Masoud, W. Li, HIF-1α pathway: role, regulation and intervention for cancer therapy, Acta Pharm. Sin. B 5 (5) (2015) 378–389.
[62] R.Y. Huang, L. Pei, Q. Liu, S. Chen, H. Dou, G. Shu, Z.X. Yuan, J. Lin, G. Peng, W. Zhang, H. Fu, Isobologram analysis: a comprehensive review of methodology and current research, Front. Pharmacol. 10 (2019) 1222.
[63] K. Strebhardt, A. Ullrich, Paul Ehrlich's magic bullet concept: 100 years of progress, Nat. Rev. Cancer 8 (6) (2008) 473–480.